



This is a repository copy of *One-part geopolymers based on thermally treated red Mud/NaOH blends*.

White Rose Research Online URL for this paper:  
<http://eprints.whiterose.ac.uk/86412/>

Version: Accepted Version

---

**Article:**

Ke, X., Bernal, S.A., Ye, N. et al. (2 more authors) (2015) One-part geopolymers based on thermally treated red Mud/NaOH blends. *Journal of the American Ceramic Society*, 98 (1). 5 - 11. ISSN 0002-7820

<https://doi.org/10.1111/jace.13231>

---

**Reuse**

Unless indicated otherwise, fulltext items are protected by copyright with all rights reserved. The copyright exception in section 29 of the Copyright, Designs and Patents Act 1988 allows the making of a single copy solely for the purpose of non-commercial research or private study within the limits of fair dealing. The publisher or other rights-holder may allow further reproduction and re-use of this version - refer to the White Rose Research Online record for this item. Where records identify the publisher as the copyright holder, users can verify any specific terms of use on the publisher's website.

**Takedown**

If you consider content in White Rose Research Online to be in breach of UK law, please notify us by emailing [eprints@whiterose.ac.uk](mailto:eprints@whiterose.ac.uk) including the URL of the record and the reason for the withdrawal request.



[eprints@whiterose.ac.uk](mailto:eprints@whiterose.ac.uk)  
<https://eprints.whiterose.ac.uk/>

## One-part Geopolymers Based on Thermally Treated Red Mud/NaOH Blends

Xinyuan Ke<sup>1,2</sup>, Susan A. Bernal<sup>2</sup>, Nan Ye<sup>1</sup>, John L. Provis<sup>2\*</sup>, Jiakuan Yang<sup>1</sup>

<sup>1</sup>*School of Environmental Science and Engineering, Huazhong University of Science & Technology, Wuhan 430074, China*

<sup>2</sup>*Department of Materials Science and Engineering, University of Sheffield, Sheffield S1 3JD, United Kingdom*

\* To whom correspondence should be addressed. Email [j.provis@sheffield.ac.uk](mailto:j.provis@sheffield.ac.uk),

Phone +44 114 222 5490, fax +44 114 222 5943

### Abstract

In this study, one-part "just add water" geopolymer binders are synthesized through the alkali-thermal activation of the red mud which is relatively rich in both alumina and calcium. The calcination of the red mud with sodium hydroxide pellets at 800°C leads to decomposition of the original silicate and aluminosilicate phases present in the red mud, which promotes the formation of new compounds with hydraulic character, including an alkali-rich phase peralkaline aluminosilicate glass and the calcium-rich phases C<sub>3</sub>A and α-C<sub>2</sub>S. The hydration of the 'one-part geopolymer' leads to the formation of zeolites and a disordered binder gel as the main reaction products, and the consequent development of compressive strengths of up to 10 MPa after 7 days of curing. These results demonstrate that red mud is an effective precursor to produce one-part geopolymer binders, via thermal and alkali-activation processes.

**Keywords:** red mud, one-part geopolymers, hydraulicity, alkali-thermal activation

## **1. Introduction**

As the demand for construction materials has increased over the past century with growth in infrastructure worldwide, there has been an increasing interest in developing lower cost, more sustainable, and high performance cements, which can meet the strength and environmental requirements of modern civil structures. Portland cement is the main binder used for concrete production; however, the cement production process emits around 850 kg of carbon dioxide per tonne of cement, which currently represents significantly more than 5% of worldwide CO<sub>2</sub> generation and will continue to increase up to 2050. This has been one of the drivers for the development and study of more environmentally friendly alternative construction materials such as alkali-activated binders<sup>1,2,3</sup>.

Alkali-activated materials derived from an aluminosilicate precursor, also referred to as ‘geopolymers’, have been the object of study in the past decades as alternative binders to traditional Portland cement, and are starting to be produced on an industrial scale and commercialized in several countries<sup>4</sup>. In most of these publications and implementations, geopolymer materials are synthesized from calcined clays such as metakaolin, fly ash derived from the coal combustion process, or metallurgical slags from the iron and steel making process<sup>5</sup>, along with an alkaline activator, to form a hardened solid with desirable cementitious properties. However, these binders can potentially be produced using a much wider range of aluminosilicate precursors, particularly those with a poorly crystalline structure, if formulated and cured appropriately<sup>3,6</sup>.

The microstructure, and consequently the performance, of geopolymers is controlled by the chemistry and mineralogy of the precursor, the type and

concentration of the alkali activator, and the curing conditions<sup>5,7</sup>. The most commonly used activators are sodium hydroxide (NaOH) and sodium silicates ( $\text{Na}_2\text{O}\cdot n\text{SiO}_2$ ). The efficiency of the activator is influenced by the available alkalinity, as this controls the initial dissolution of the precursor and the consequent condensation reactions to form the insoluble aluminosilicate compounds<sup>8,9,10</sup>. The alkaline activator can be included in the mix as a liquid solution or as a powder mixed with the solid raw material<sup>11</sup>; it is usually included as a highly alkaline solution.

However, it is more desirable and convenient for commercial usage to develop one-part "just add water" geopolymers that can be used in a similar way to Portland cement. Studies focused on synthesis of one-part geopolymer are relatively limited in this growing area of research<sup>12, 13, 14, 15, 16</sup>, although some have reported mechanical strength comparable with geopolymers produced using liquid alkaline solutions<sup>13, 15</sup>. Nonetheless, the mineralogy and formation mechanism of reaction of these one-part geopolymer precursors requires further and detailed research.

One of the technical barriers facing production of one-part geopolymers is the initial dissolution of the aluminosilicate precursor, which generally requires a highly alkaline environment with a minimum pH of 11 to initiate. By adding alkaline solutions to activate the geopolymer, an alkaline environment with a pH of 14 can be easily achieved. Conversely, when using powdered activators and adding water to the systems, the solution moves more slowly from neutral to higher alkalinity, slowing down the kinetics of reaction<sup>5</sup>. Therefore, one plausible way to produce one-part geopolymer is to synthesize mixes with a precursor pre-containing high contents of alkalis that can be easily leachable when the water is added.

Red mud is an alkaline residue (pH between 9.2 to 12.8 in untreated residue liquor of red mud<sup>17</sup>) derived from alumina extraction via the Bayer process, where bauxite

ore is digested in NaOH solutions. After the majority of the Al is recovered, the red mud contains a significant quantity of entrained NaOH. The material is red due to its content of Fe oxides, but is also relatively rich in Si from impurities in the bauxite, as well as containing some residual Al, if the process is not fully efficient. The worldwide annual production of red mud is estimated at 120 million tonnes/year, which makes its disposal an issue of great environmental importance<sup>18</sup>. Currently this material is underutilized, and even though its chemical and mineralogical compositions vary widely depending on the source of bauxite and the production process<sup>19, 20</sup>, it has desirable properties for the production of geopolymer materials.

The geopolymerization of red mud as a sole precursor has generally been limited in success, due to the low available Al content of the red mud sources which have generally been tested; however, the use of more Al-rich red mud<sup>21</sup> and incorporation of supplementary Al sources such as metakaolin<sup>22</sup> or fly ash<sup>23, 24</sup> contributes to enhance the mechanical strength development. The inclusion of Ca-rich materials such as slag has also proven to have a positive impact in the compressive strength of red mud based geopolymers<sup>25, 26, 27</sup>. A recent study has shown that thermal treatment is an effective way to make red mud more reactive for production of geopolymers, though liquid alkaline silicate solutions were still required<sup>27, 28</sup>.

In this study, a series of "just add water" geopolymers are produced from red mud through alkali-thermal pre-processing of the red mud, then reaction with water to form a hardened solid. The microstructure and mineralogy of the alkali-thermally treated red mud, before and after addition of water, are studied through X-ray diffraction, infrared spectroscopy, scanning electron microscopy (SEM), and determination of the compressive strength of the hydrated geopolymer samples as a function of time.

## 2. Experimental program

### 2.1. Materials characterization

The red mud used in this study was supplied by the alumina plant of CHALCO Henan Branch, Zhengzhou, China, and was dried and stored at room temperature. The chemical composition of the red mud is given in Table 1. These results indicate that the red mud is rich in Al, and also has a significant content of Ca, which make it suitable for production of geopolymers. Commercial sodium hydroxide pellets from Sinopharm Chemical Reagent Co., Ltd with NaOH  $\geq 96.0\%$  were used as an additional alkali source.

**Table 1.** Chemical composition of the red mud and slag used, determined via X-ray fluorescence analysis. LOI is loss on ignition at 1000°C

#### 2.1.1. Alkali-thermal pre-activation of red mud

The red mud was sieved ( $-300\ \mu\text{m}$ ), and then dried in an oven at 45°C for 24 hours prior to thermal treatment. The dried red mud was then mixed with 5 wt.%, 10 wt.% and 15 wt.% of Na<sub>2</sub>O, added as sodium hydroxide. The dry mix was ground in a ring mill for 2 min to assure good blending of the powders. Afterwards, the powder blends with different contents of sodium hydroxide were heated to 800°C, at a heating rate of 5 °C/min, and held at 800°C for an hour before cooling naturally in the furnace to room temperature (25°C). As a reference to compare the effect of incorporated alkali, the red mud was also treated under same thermal conditions without alkali addition (samples labeled 0% Na<sub>2</sub>O). The cooled samples were sieved ( $-300\ \mu\text{m}$ ) again to minimize potential effects of particle dissolution in the geopolymerization.

This treatment temperature was selected considering the thermogravimetry results

of red mud from this same source as reported by Ye et al.<sup>27</sup>, where it was identified that the dehydroxylation and decarbonation of all of the crystalline compounds present takes place at temperatures below 800°C. It has previously been suggested<sup>29</sup> that the thermal behavior of red mud could be modified by the inclusion of alkalis, shifting the peaks of dehydroxylation and decarbonation towards lower temperature, and preliminary testing of these samples showed that both mechanisms will take place below 800°C.

### **2.1.2. Red mud based one-part geopolymer**

Pastes specimens were then prepared by adding water to the solid with a water/solid ratio of 0.6. After mixing in the Hobart mixer for 4 min, the fresh pastes were cast into 40×40×40 mm molds and sealed with polymer film. All the specimens were cured at 20 ± 1°C and a relative humidity of 95%, in a controlled humidity chamber. After 1, 3, 7 and 28 days of curing, the compressive strength was tested. The crushed samples were then immersed in acetone for 24 hours before being oven dried at 60°C, and pulverized for analysis. It is worth noting that the red mud binder pre-heated without alkali addition showed no hydraulicity even after 28 days of curing; therefore, only limited characterization result of this sample (denoted RM800-0%Na<sub>2</sub>O) are presented.

## **2.2. Analytical methods**

X-ray diffractometry and Fourier transform infrared spectroscopy were used to analyze the anhydrous red mud binders. Similar techniques were used to analyze the hydrated geopolymer binders, along with SEM analysis of fracture sections. The equipment and conditions used for this analysis are described below.

- X-ray diffraction was conducted using a D/Max-3B X-ray diffractometer with

a scan step size of 0.0167 degrees per step, operating with a voltage and current of 40 kV and 40 mA respectively, and Ni-filtered Cu-K $\alpha$  radiation.

- Fourier transform infrared spectroscopy was carried out by the KBr method in a VERTEX 70 spectrometer, in a scanning range of 400 to 4000 cm<sup>-1</sup>.
- Compressive strength of the cubes of hardened geopolymer paste was conducted in a universal testing machine (YAW-300E), with a loading rate of 144 kN/min. Each value reported corresponds to the average of two samples.
- SEM images were obtained in a Sirion 2000 Field Emission Scanning Electron Microscope (FSEM), examining gold coated fracture sections of the geopolymers produced, operating in the vacuum mode and using an acceleration voltage of 20 keV.

### 3. Results and discussion

#### 3.1. Characterization of the anhydrous red mud binder

##### 3.1.1. X-ray Diffraction

The mineralogical analysis of the unreacted red mud has been conducted by X-ray diffraction (Fig. 1, Unreacted RM), where the main crystalline compounds identified are the Al-rich and alkali-rich phases gibbsite (Al(OH)<sub>3</sub>, powder diffraction file (PDF) #00-033-0018), cancrisilite (Na<sub>7</sub>(Al<sub>5</sub>Si<sub>7</sub>O<sub>24</sub>)CO<sub>3</sub>·3H<sub>2</sub>O, PDF #00-046-1381) and muscovite (KAl<sub>2</sub>Si<sub>3</sub>AlO<sub>10</sub>(OH)<sub>2</sub>, PDF #00-007-0025); the Ca-containing phases hydrogarnet (Ca<sub>2.93</sub>Al<sub>1.97</sub>(Si<sub>0.64</sub>O<sub>2.56</sub>)(OH)<sub>9.44</sub>, PDF #01-077-1713) and calcite (CaCO<sub>3</sub>, PDF #00-005-0586), along with traces of hematite (Fe<sub>2</sub>O<sub>3</sub>, PDF #01-072-0469). Cancrisilite has the framework structure of cancrinite but a higher Si/Al ratio of around 7:5 (rather than 1:1 in cancrinite) and a largely disordered arrangement of Si and Al<sup>30</sup>.



**Fig. 1** X-ray diffractograms of unreacted red mud and red mud binders prepared by thermally treated at 800°C incorporated with different amount of alkali. *S* - cancrisilite, *H* - hydrogarnet, *G* - gibbsite, *M* - muscovite, *a* - calcite, *F* - hematite, *N* - nepheline, *G<sub>e</sub>* - gehlenite, *P* and *P<sub>α</sub>* – disordered peralkaline aluminosilicate, *C* – Ca-substituted cancrinite, *T* - tricalcium aluminate, *A* – hexagonal CAS<sub>2</sub>, *B* - belite.

The crystalline phases identified in the unreacted red mud decomposed after thermal treatment at 800°C for 1 hour; this is associated with dehydration, dehydroxylation and decarbonation process. Upon thermal processing in absence of alkalis (Fig. 1), the alkali-rich crystalline phase nepheline ((K,Na)AlSiO<sub>4</sub>, similar to PDF #01-076-1858 or PDF #01-088-1191) and the Ca-rich phase gehlenite (Ca<sub>2</sub>Al<sub>2</sub>SiO<sub>7</sub>, PDF#00-009-0216 ) are identified. Nepheline is the dehydration and decarbonation product of the cancrisilite present in the unreacted red mud <sup>31</sup>. Cancrisilite and cancrinite exhibit similar two-step decomposition processes upon thermal treatment: first dehydration, then decarbonation (sometimes along with dehydroxylation if hydroxyl groups are available)<sup>30</sup>.

The dehydration process of cancrinite is usually complete at 600°C, while the release of CO<sub>2</sub> starts at 500°C and is complete by 1300°C <sup>32, 33, 34</sup>. Although the range of temperatures at which these decomposition processes occur is dependent on the exact chemical composition of the cancrinite, the formation of nepheline is always identified<sup>31, 32, 35</sup>, consistent with the results shown in Fig. 1.

Gehlenite is most likely derived from the chemical interaction between thermally decomposed hydrogarnet (identified in the unreacted red mud, Fig 1) and the available

silicate and alumina derived from the other compounds present in the unreacted red mud, such as muscovite and gibbsite, which are no longer observed in the thermally treated red mud. The reflections assigned to hematite remain unchanged after thermal treatment at 800°C.

When alkali is incorporated during the thermal pre-activation process, instead of forming nepheline a new Na-rich phase (a partially disordered peralkaline aluminosilicate,  $[\text{Na}_2\text{O}]_x[\text{NaAlO}_2]_y[\text{NaAlSiO}_4]$ , represented by phase P in Fig. 1, PDF# 01-076-2385 when  $x>0, y=0$ ; represented by phase  $P_\alpha$ , PDF# 00-049-0004 when  $x=0, y>0$ , both described below as Na-aluminosilicate for brevity) is identified, along with a Ca-substituted cancrinite phase ( $\text{Na}_6\text{Ca}_{1.5}\text{Al}_6\text{Si}_6\text{O}_{24}(\text{CO}_3)_{1.6}$ , PDF# 00-034-0176). Both of these phases are modifications of cancrisilite and belong to the cancrinite group<sup>30, 36</sup>. The crystal structures of members from this group contain vacancies and large channels in the cancrinite framework, especially some accessible 12-rings, which allow the ingress of excess cations such as  $\text{Na}^+$  and  $\text{Ca}^{2+}$ ; or even larger cluster ions such as  $[\text{Na}\cdot\text{H}_2\text{O}]^{+33}$ .

In this study, the  $[\text{Na}\cdot\text{H}_2\text{O}]^+$  clusters are supplied by the incorporation of sodium hydroxide, which melts and is partially ionized in the flux state when the mix reaches a temperature of around 319°C<sup>37</sup>. The availability of  $\text{Ca}^{2+}$  could be due to both decomposed calcite and to decomposition products of hydrogarnet. Capture of both  $[\text{Na}\cdot\text{H}_2\text{O}]^+$  clusters and  $\text{Ca}^{2+}$  can happen simultaneously; however, a higher  $\text{Na}^+$  concentration increases the driving force for the incorporation of  $[\text{Na}\cdot\text{H}_2\text{O}]^+$  clusters and thus enhances alkali inclusion in the crystalline aluminosilicates during the thermal activation process, and the consequent decomposition of cancrisilite towards formation of the peralkaline Na-aluminosilicate. Due to the availability of the non-framework sites for uptake of extra cations in the cancrinite structure, the excessive incorporation

of alkali reduced the incorporation of  $\text{Ca}^{2+}$ , consistent with the results in Fig. 1 where with up to 15% alkali addition the Ca-cancrinite is no longer identified.

The thermal-alkali pre-treatment also influences the Ca-rich phases. Instead of gehlenite, it is possible to identify tricalcium aluminate ( $\text{Ca}_3\text{Al}_2\text{O}_6$ , PDF#00-006-0495, abbreviated  $\text{C}_3\text{A}$ ), a metastable hexagonal calcium aluminosilicate with some Fe substitution in its diphylosilicate structure<sup>38, 39</sup>, approximately  $\text{CaAl}_{2-x}(\text{Al,Fe})_x\text{Si}_2\text{O}_8$ , similar to PDF#00-031-0248, abbreviated  $\text{CAS}_2$ ) and belite ( $\alpha_L'$ - $\text{Ca}_2\text{SiO}_3$ , PDF#00-033-0303) in red mud binders including 10 wt.% and 15 wt.% of alkali, also associated with the decomposition of hydrogarnet<sup>40</sup>. The formation of these compounds is beneficial for the reaction of the one-part geopolymers assessed here, as these are known as hydraulic cementitious phases that exhibit high reactivity when blended with water. The disordered hematite is no longer identified in red mud binders with 15 wt.% alkali, possibly due to substitution of Fe into the aluminate and/or silicate phases described above.

### **3.1.2. Fourier Transform Infrared Spectroscopy**

Fig. 2 shows infrared spectra of the thermal-alkali pre-activated red mud powders. In the untreated red mud spectrum, bands at  $3430\text{ cm}^{-1}$  and  $1631\text{ cm}^{-1}$  correspond to the stretching and bending vibration modes of O-H in hydroxyl groups, respectively, and are attributed to water present in the raw material<sup>41</sup>. The band at  $3622\text{ cm}^{-1}$  and  $3525\text{ cm}^{-1}$  are assigned to the surface hydroxyl group of lepidocrocite ( $\gamma\text{-FeO(OH)}$ )<sup>42</sup> and gibbsite<sup>43</sup>. Iron oxyhydroxides are commonly present in untreated red mud<sup>17, 44, 45</sup>; however, they have not been identified by XRD, neither in the untreated red mud nor in the thermally activated binders, which suggests that the

poorly crystallized iron in this material is most likely present as a  $\gamma$ -FeO(OH) type phase.

This suggestion is supported by the fact that the dehydroxylation of both gibbsite and lepidocrocite would be completed before 600°C<sup>46, 47</sup>, and the bands at 3622 cm<sup>-1</sup> and 3525 cm<sup>-1</sup> are no longer identified in the FTIR spectra of the red mud after thermal treatment. Bands between 1500 cm<sup>-1</sup> and 1300 cm<sup>-1</sup> are related to stretching vibration of carbonate groups present in the calcite and cancrinite. Specifically, the band at 1504 cm<sup>-1</sup> corresponds to carbonate-bearing cancrinite groups<sup>33</sup>.

**Fig. 2** FTIR spectra of unreacted red mud and alkali-incorporated thermally pre-activated red mud.

After the thermal pre-treatment at 800°C, the relative intensities of bands related to hydroxyl and carbonate groups are significantly reduced due to the dehydration/dehydroxylation of crystalline phases; however, these peaks re-emerge with the incorporation of higher contents of alkalis in thermal processing. This phenomenon is caused by the absorption of CO<sub>2</sub> and H<sub>2</sub>O from the ambient atmosphere during (or prior to) analysis, as the red mud binders are highly alkaline and hygroscopic.

The vibration modes between 900 cm<sup>-1</sup> and 1200 cm<sup>-1</sup> are assigned to stretching vibrations of Si-O-T bonds, the positions of which are influenced by two aspects: the amount of Al substituted in the tetrahedral (T) site connected with the bridging oxygen, and the number of bridging vs. non-bridging oxygens<sup>41, 48, 49</sup>. Substitution away from a pure SiO<sub>2</sub> network leads to the observed shift to lower wavenumbers of this vibration

band, as a result of the decreased bonding energy upon substitution in this system. Since the hydrolysis of Si-O-Al bonds and depolymerization of the glassy phase both favor the release of Al and Si from the aluminosilicate sources at the early stage of dissolution, a shift in vibration bands towards lower wavenumbers, within this range, is proposed to indicate better potential geopolymerization performance of the binder<sup>5</sup>.

Bands appearing between 750-550 cm<sup>-1</sup> are related to vibration of silicate ring structures, and a reduction of the wavenumber within this region is associated with a reduced number of bridging oxygens in the corresponding ring structure<sup>50</sup>. In this study, bands at about 690 cm<sup>-1</sup>, 622 cm<sup>-1</sup> and 578 cm<sup>-1</sup> are assigned to vibration of 4-membered and 6-membered rings from the cancrinite  $\epsilon$ -cage framework<sup>34</sup>.

As the amount of alkali incorporated during the thermal process increases, the peaks between 900 cm<sup>-1</sup> and 1200 cm<sup>-1</sup> shift towards lower wavenumber as the main peak in this region shifts from 998 cm<sup>-1</sup> to 985 cm<sup>-1</sup>. The increase of Al in the Si-O-T bonds raises the negative charge on the framework, increasing its ability to incorporate alkali cations in the channels for charge balancing<sup>51</sup>. The broad and overlapping peaks between this region are also the result of deformed bonding structures caused by cations like Ca<sup>2+</sup> and the [Na•H<sub>2</sub>O]<sup>+</sup> cluster becoming incorporated into the channel or vacancies in cancrinite cage frameworks<sup>52</sup>. Additionally, a shoulder at 870 cm<sup>-1</sup> that assigns to asymmetric stretching of the Al-O bonds in AlO<sub>4</sub> tetrahedra appears, associated with the C<sub>3</sub>A phase in the red mud binder with 10% alkali, and the Na-aluminosilicate phase (P <sub>$\alpha$</sub> [NaAlO<sub>2</sub>]<sub>y</sub>[NaAlSiO<sub>4</sub>]) with 15% alkali, both identified from the XRD analysis in Fig. 1.

The thermal treatment promotes a shift in the bands from 578 cm<sup>-1</sup> and 622 cm<sup>-1</sup> towards higher wavenumber, as the decreasing number of members in the ring structure is also related to a reduced number of bridging oxygens. The broad vibration

mode appearing between  $630\text{ cm}^{-1}$  and  $690\text{ cm}^{-1}$  is associated with the existence of a range of deformed 4-membered silicate ring structures, indicating a disordered state within these solid powders.

## 3.2. Reaction and hardening of red mud based one-part geopolymers

### 3.2.1. X-ray Diffraction

Fig. 3 shows the crystalline phases identified in red mud based one-part geopolymers after 7 and 28 days of curing. Note that no mechanical strength was developed by RM800-5%Na<sub>2</sub>O after 7 days of curing, therefore the related XRD results are not shown here. The alkali-rich Na-aluminosilicate phase, and the Ca-rich phases C<sub>3</sub>A and hexagonal CAS<sub>2</sub> are no longer identified. The cancrinite and hematite present in some of the anhydrous precursors stayed almost unchanged after hydration.

**Fig. 3** X-ray diffractograms of one-part geopolymer synthesised from alkali-thermal pre-activated red mud binder with (A) 15%Na<sub>2</sub>O, (B) 10%Na<sub>2</sub>O, (C) 5%Na<sub>2</sub>O over different days of curing. P and P<sub>α</sub> - peralkaline aluminosilicate, C - cancrinite, B - belite, F - hematite, Z - zeolite NaA, H - hydrogarnet, T - tricalcium aluminate, A – hexagonal CAS<sub>2</sub>.

The peralkaline phases with compositions described as (Na<sub>2</sub>O)<sub>x</sub>(NaAlO<sub>2</sub>)<sub>y</sub>(NaAlSiO<sub>4</sub>) appear to be the main hydraulic components in red mud-based geopolymer binders. The Si-O-T bonds in the peralkaline phases hydrolyze after contact with water, which is rapidly made alkaline by the release of alkalis from the material structure. As a result, the remaining Al<sup>3+</sup> and Na<sup>+</sup> are released from the

framework structure to charge balance the OH<sup>-</sup> released by the hydrolysis process. The hydrolysis of Si-O-T bonds also breaks the oxygen bridges in the aluminosilicate structural frameworks, generating the Si-OH silicate structures that can later polymerize<sup>53, 54, 55</sup>. The dissolution mechanism of the peralkaline phases in water<sup>54, 55</sup> is analogous to the early stage dissolution mechanism of a one-part geopolymer illustrated by Duxson & Provis<sup>5</sup>. The hydration product of this crystalline phase is a disordered aluminosilicate gel structure, also referred to as geopolymer gel or N-A-S-(H) gel, which is the main strength-giving phase in aluminosilicate geopolymers<sup>3</sup>.

Geopolymer gel units are similar in nature to the composite building units which comprise zeolites<sup>56, 57</sup>. Under high-alkali conditions, the geopolymer gel units would transform to zeolites at advanced times of curing, and the specific types of zeolite formed will depend on the starting material and the chemistry of the pore solution<sup>56, 58, 59</sup>. Zeolite NaA (approximately Na<sub>2</sub>Al<sub>2</sub>Si<sub>1.85</sub>O<sub>7.7</sub>·5.1H<sub>2</sub>O, PDF# 00-038-0241) is identified only after 28 days of curing; therefore, it is highly possible that the dissolved peralkaline aluminosilicate initially formed disordered geopolymer gel units that transform to zeolite NaA at advanced times of curing. This phase has also been identified in one-part geopolymers made from a solid mixture of geothermal silica and sodium aluminate<sup>12</sup>, possibly via a similar mechanism.

If the samples are not perfectly sealed, CO<sub>2</sub> from the ambient atmosphere will react with the high alkali pore solution and form carbonate. When there is CO<sub>3</sub><sup>2-</sup> available in the pore solution, zeolite NaA can transform to carbon-bearing cancrinite<sup>60</sup>. Matrixes with higher alkalinity are more tend to carbonate. In Fig. 3, cancrinite is observed in RM800-15%Na<sub>2</sub>O after 28 days of curing, while in RM800-10%Na<sub>2</sub>O zeolite NaA is identified. No crystalline zeolite phase is identified in the hydrated

RM800-5%Na<sub>2</sub>O paste due to a lower-alkali activation condition and therefore a much slower reaction rate within the timeframe studied here.

The hydration process of the Ca-rich phases formed through thermal decomposition of hydrogarnet are likely to be similar to that of a Portland cement binder<sup>61</sup>. The main hydration product of these Ca-rich phases after 7 days is hydrogarnet, Ca<sub>3</sub>Al<sub>1-x</sub>(Fe,Al)<sub>x</sub>(SiO<sub>4</sub>)<sub>3-y</sub>·(OH)<sub>4y</sub>, with the degree of Fe substitution depending on the availability of Fe<sup>3+</sup> in the solid solution system, associated with the hydration of C<sub>3</sub>A in the hydrated RM800-10%Na<sub>2</sub>O binder, and additionally the hydration of both hexagonal CAS<sub>2</sub> and belite in the hydrated RM800-15%Na<sub>2</sub>O binder. These hydrate phases are strength-giving phases in calcium aluminate cement, and are also common secondary phases in geopolymers<sup>2</sup>.

### 3.2.2. *Fourier Transform Infrared Spectroscopy*

Fig. 4 shows the FTIR spectra of the hydrated red mud one-part geopolymer at different times of curing. High intensity bands at 3443 cm<sup>-1</sup> and 1655 cm<sup>-1</sup> are identified due to the stretching and bending vibrations of H-OH bonds in chemically bonded water, indicating the formation of hydration products. The intensities of these bands rise significantly after 7 days of curing but decrease slightly after 28 days. This suggests that the hydration process of the red mud binder proceeds quickly during the first 7 days; however, some of the hydration products dehydrate (or densify and release water into the pores) at a more advanced time of curing (28 days).

**Fig. 4** *FTIR spectra of one-part geopolymer generated from R800-10%Na<sub>2</sub>O at different times of curing.*



The strong bands at  $1458\text{ cm}^{-1}$  and the weak bands at  $866\text{ cm}^{-1}$  are assigned to the anti-symmetric stretching vibration and out-of-plane bending of the C=O bond in carbonate. The identification of these two bands is attributed to the partial atmospheric carbonation of the matrix, either during curing or analysis.

The overlapped bands centered at around  $989\text{ cm}^{-1}$  in the anhydrous precursor shift towards  $1000\text{ cm}^{-1}$  upon hydration, and forming a narrow band, associated with the Si-O-Al bonds in N-A-S-H gel and zeolite NaA. The shoulder initially present at  $870\text{ cm}^{-1}$  is not identified after hydration. The bands between  $550\text{ cm}^{-1}$  and  $700\text{ cm}^{-1}$  ( $690\text{ cm}^{-1}$ ,  $624\text{ cm}^{-1}$  and  $577\text{ cm}^{-1}$ ) in the anhydrous binder are replaced by a peak at  $563\text{ cm}^{-1}$  upon hydration, which is assigned to the out of plane bending vibration of Si-O-T bonds in the double ring structure in zeolite NaA. The changes in these vibration bonds are possibly associated with crosslinking of the geopolymer gel. The band at  $3661\text{ cm}^{-1}$  that was assigned in the red mud spectrum to the vibration of hydroxyl groups in hydrogarnet reappears upon hydration, consistent with the XRD results (Fig. 3).

### **3.2.3. Compressive strength**

The compressive strength development of the one-part geopolymer produced from different red mud based binders is shown in Fig. 5. The paste made from RM800-5%Na<sub>2</sub>O did not harden in the first 7 days of curing, but gradually gained strength in the following 14 days. The slow reaction taking place in the red mud binder RM800-5%Na<sub>2</sub>O is due to the low content of hydraulic reacting phases, particularly peralkaline aluminosilicate, present in the binder. The red mud binder produced with 15 wt.% alkali hardened quickly and developed strength after 24 hours, and reached a maximum in its strength at 7 days, beyond which there was a significant strength loss, as discussed below. The reaction of the red mud binder activated with 10 wt.% alkali is

slower compared with the system with higher alkali content; however, an optimum 7 day strength of 9.8 MPa was reached, higher than that of the red mud binder with 15 wt.% alkali.

*Fig. 5 Compressive strengths of red based one-part geopolymers produced with different activator doses as a function of the time of curing.*

Red mud alone has not been successfully used as a precursor for synthesis of either one-part or two-part geopolymers, as partial replacement by high calcium or alumina sources such as slag and fly ash has been required in the literature reports of this process<sup>23, 24, 27</sup>. Thus, the early stage strength gained by the red mud based one-part geopolymer developed from RM800-10%Na<sub>2</sub>O and RM800-15%Na<sub>2</sub>O demonstrates the advantages of the alkali-thermal pre-activation process to enhance the reactivity of this material as a sole geopolymer precursor.

However, there is a significant engineering downside observed in Fig. 5, as the red mud based one-part geopolymers synthesized in this study exhibited a significant decrease in compressive strength during the second and third weeks of curing. This can be a consequence of the degradation of the matrix through processes including dehydration, carbonation and efflorescence, as one of the reasons that usually influences the morphology of microstructure and undermines the strength of geopolymer. In this study, dehydration and partial carbonation of the geopolymer matrix have been observed from FTIR analysis (Fig. 4). Formation of efflorescence products was also observed, as white crystalline alkaline deposits were observed on the surface of the paste cube samples after 14 days of curing. This phenomenon has also

been observed in some metakaolin-based geopolymers<sup>62</sup> and was associated with potential depolymerization of the geopolymer gel at advanced times of curing, as a consequence of the loss of the charge balancing alkaline cations from the gel, which could conceivably result in loss of mechanical strength.

It is important to note that Najafi Kani et al.<sup>63</sup> have demonstrated that blending minor percentages of an additional Al source with the geopolymer binder can lead to reduced efflorescence in these materials. This suggests that better control of efflorescence, and potentially improved compressive strength retention, could be achieved through optimization of the formulations of the one-part geopolymers produced in this study. Nonetheless, the initial strengths generated by the materials studied here can certainly stand as proof-of-concept for the approach followed.

#### **3.2.4. Scanning electron microscopy (SEM)**

Fig. 6 shows the SEM images of the fracture surface of the red mud one-part geopolymer after strength testing. In Fig. 6A, the semi-crystallized plates corresponding to zeolite type phases present are surrounded by the nano-scale gel particles. The one-part geopolymer has a significantly low Si/Al ratio (about 0.7 in the starting material), and the microstructure of this geopolymer is consistent with the trends reported by Duxson et al.<sup>64</sup>, who identified in metakaolin based geopolymers that a Si/Al ratio lower than 1.4 promotes a highly porous microstructure with unreacted particles surrounded by geopolymer gel. After 28 days of curing, the plate-shaped particles are converted to more refined crystals; however, the overall microstructure is still porous and heterogeneous as shown in Fig. 6B.

**Fig. 6** SEM micrographs of the fracture surface of one-part geopolymer generated from R800-10%Na<sub>2</sub>O after (A) 7 and (B) 28 days of curing.

#### 4. Conclusions

The incorporation of alkali during the thermal activation of an Al-rich red mud favors the formation of hydraulic phases: peralkaline Na-aluminosilicate, C<sub>3</sub>A and  $\alpha_1$ '-C<sub>2</sub>S. The formation of Na-rich aluminosilicate salts provides sufficient alkalis for the dissolution process to take place upon addition of water alone, and improves the reactivity of the red mud binder by increasing the availability of Al during the initial gel formation process and subsequent ongoing condensation reactions.

The strength development of this red mud based one-part geopolymer is limited by the excess of alkalis in the system and efflorescence problems; however, compared to previous activation methods, the alkali-thermal pre-activation process described here can certainly enhance the activity of red mud to produce sustainable cement.

#### Acknowledgements

The investigation was supported in part by the New Century Excellent Talents Project of the Ministry of Education (China) (NCET-09-0392). The participation of JLP and SAB was funded by the University of Sheffield.

## References

1. J. S. J. Van Deventer, J. L. Provis, P. Duxson, and D. G. Brice, "Chemical Research and Climate Change as Drivers in the Commercial Adoption of Alkali Activated Materials," *Waste Biomass Valoriz.*, **1**[1] 145-55 (2010).
2. J. L. Provis, "Geopolymers and Other Alkali Activated Materials: Why, How, and What?," *Mater. Struct.*, **47** 11-25 (2014).
3. J. L. Provis and S. A. Bernal, "Geopolymers and Related Alkali-Activated Materials," *Annu. Rev. Mater. Res.* in press, DOI 10.1146/annurev-matsci-070813-113515 (2014).
4. J. Provis, D. Brice, A. Buchwald, P. Duxson, E. Kavalerova, P. Krivenko, C. Shi, J. J. Deventer, and J. A. L. M. Wiercx, "Demonstration Projects and Applications in Building and Civil Infrastructure," pp. 309-38. in *Alkali-Activated Materials: State-of-the-Art Report, RILEM TC 224-AAM*. Edited by J. L. Provis and J. S. J. Van Deventer. Springer/RILEM, Dordrecht, 2014.
5. P. Duxson and J. L. Provis, "Designing Precursors for Geopolymer Cements," *J. Am. Ceram. Soc.*, **91**[12] 3864-69 (2008).
6. H. Xu and J. S. J. van Deventer, "Geopolymerisation of Multiple Minerals," *Miner. Eng.*, **15**[12] 1131-39 (2002).
7. M. C. G. Juenger, F. Winnefeld, J. L. Provis, and J. Ideker, "Advances in Alternative Cementitious Binders," *Cem. Concr. Res.*, **41**[12] 1232-43 (2011).

8. A. Fernández-Jiménez and F. Puertas, "Effect of Activator Mix on the Hydration and Strength Behaviour of Alkali-Activated Slag Cements," *Adv. Cem. Res.*, **15**[3] 129-36 (2003).
9. C. Shi, "On the State and Role of Alkalis During the Activation of Alkali-Activated Slag Cement," in *Proceedings of the 11th International Congress on the Chemistry of Cement*, CD-ROM, 2003.
10. S. Song, D. Sohn, H. M. Jennings, and T. O. Mason, "Hydration of Alkali-Activated Ground Granulated Blast Furnace Slag," *J. Mater. Sci.*, **35** 249-57 (2000).
11. K. H. Yang and J. K. Song, "Workability Loss and Compressive Strength Development of Cementless Mortars Activated by Combination of Sodium Silicate and Sodium Hydroxide," *J. Mater. Civ. Eng.*, **21**[3] 119-27 (2009).
12. A. Hajimohammadi, J. L. Provis, and J. S. J. van Deventer, "One-Part Geopolymer Mixes from Geothermal Silica and Sodium Aluminate," *Ind. Eng. Chem. Res.*, **47**[23] 9396-405 (2008).
13. A. Hajimohammadi, J. L. Provis, and J. S. J. van Deventer, "Effect of Alumina Release Rate on the Mechanism of Geopolymer Gel Formation," *Chem. Mater.*, **22**[18] 5199-208 (2010).
14. A. Hajimohammadi, J. L. Provis, and J. S. J. van Deventer, "The Effect of Silica Availability on the Mechanism of Geopolymerisation," *Cem. Concr. Res.*, **41**[3] 210-16 (2011).

15. D. Feng, J. L. Provis, and J. S. J. van Deventer, "Thermal Activation of Albite for the Synthesis of One-Part Mix Geopolymers," *J. Am. Ceram. Soc.*, **95**[2] 565-72 (2012).
16. D. Koloušek, J. Brus, M. Urbanova, J. Andertova, V. Hulinsky, and J. Vorel, "Preparation, Structure And Hydrothermal Stability of Alternative (Sodium Silicate-Free) Geopolymers," *J. Mater. Sci.*, **42**[22] 9267-75 (2007).
17. M. Grafe, G. Power, and C. Klauber, "Bauxite Residue Issues: III. Alkalinity and Associated Chemistry," *Hydrometallurgy*, **108**[1-2] 60-79 (2011).
18. Y. Pontikes and G. N. Angelopoulos, "Bauxite Residue in Cement and Cementitious Applications: Current Status and A Possible Way Forward," *Resour. Conserv. Recycl.*, **73** 53-63 (2013).
19. X. M. Liu and N. Zhang, "Utilization of Red Mud in Cement Production: A Review," *Waste Manag. Res.*, **29**[10] 1053-63 (2011).
20. A. Atasoy, "The Comparison of the Bayer Process Wastes on the Base of Chemical and Physical Properties," *J. Thermal Anal. Calorim.*, **90**[1] 153-58 (2007).
21. A. S. Wagh and V. E. Douse, "Silicate Bonded Unsintered Ceramics of Bayer Process Waste," *J. Mater. Res.*, **6**[5] 1094-102 (1991).
22. D. D. Dimas, I. P. Giannopoulou, and D. Panias, "Utilization of Alumina Red Mud for Synthesis of Inorganic Polymeric Materials," *Miner. Proc. Extract. Metall. Rev.*, **30**[3] 211-39 (2009).

23. S. Srikanth, A. K. Ray, A. Bandopadhyay, B. Ravikumar, and A. Jha, "Phase Constitution During Sintering of Red Mud and Red Mud-Fly Ash Mixtures," *J. Am. Ceram. Soc.*, **88**[9] 2396-401 (2005).
24. X. Chen, A. Lu, and G. Qu, "Preparation and Characterization of Foam Ceramics from Red Mud and Fly Ash using Sodium Silicate as Foaming Agent," *Ceram. Int.*, **39**[2] 1923-29 (2013).
25. Z. Pan, Y. Fang, and C. Zhao, "Research on Alkali Activated Slag-Red Mud Cement Preparation," *Bull. Chin. Ceram. Soc.*, **18**[3] 34-39 (1999).
26. Z. H. Pan, D. X. Li, J. Yu, and N. R. Yang, "Properties and Microstructure of the Hardened Alkali-Activated Red Mud-Slag Cementitious Material," *Cem. Concr. Res.*, **33**[9] 1437-41 (2003).
27. N. Ye, J. Yang, X. Ke, J. Zhu, Y. Li, C. Xiang, H. Wang, L. Li, and B. Xiao, "Synthesis and Characterization of Geopolymer from Bayer Red Mud with Thermal Pretreatment," *J. Am. Ceram. Soc.* DOI: 10.1111/jace.12840 (2014).
28. N. Ye, J. Zhu, J. Liu, Y. Li, X. Ke, and J. Yang, "Influence of Thermal Treatment on Phase Transformation and Dissolubility of Aluminosilicate Phase in Red Mud," *Mater. Res. Soc. Symp. Proc.* **1488**, doi:10.1557/opl.2012.1546 (2012).
29. A. Alp and M. S. Goral, "The Influence of Soda Additive on the Thermal Properties of Red Mud," *J. Thermal Anal. Calorim.*, **73**[1] 201-07 (2003).
30. L. P. Ogorodova, L. V. Mel'chakova, M. F. Vigasina, L. V. Olyshich, and I. V. Pekov, "Cancrinite and Cancrisilite in the Khibina-Lovozero Alkaline Complex: Thermochemical and Thermal Data," *Geochem. Int.*, **47**[3] 260-67 (2009).



31. J. Felsche and S. Luger, "Phases and Thermal Decomposition Characteristics of Hydro-sodalites  $\text{Na}_{6+x}[\text{AlSiO}_4]_6(\text{OH})_x \cdot n\text{H}_2\text{O}$ ," *Thermochim. Acta*, **118**[0] 35-55 (1987).
32. J. C. Buhl, "Synthesis and Characterization of the Basic and Non-Basic Members of the Cancrinite-Natrodavayne Family," *Thermochim. Acta*, **178**[0] 19-31 (1991).
33. L. V. Olysyh, M. F. Vigasina, L. V. Melchakova, L. P. Ogorodova, I. V. Pekov, and N. V. Chukanov, "Thermal Evolution and Thermochemistry of the Cancrinite-Group Carbonate-Oxalate Mineral," *Geochem. Int.*, **49**[7] 731-37 (2011).
34. I. Hassan, S. M. Antao, and J. B. Parise, "Cancrinite: Crystal Structure, Phase Transitions, and Dehydration Behavior with Temperature," *Am. Mineral.*, **91**[7] 1117-24 (2006).
35. P. Lambert, C. L. Page, and N. R. Short, "Pore Solution Chemistry of the Hydrated System Tricalcium Silicate/Sodium Chloride/Water," *Cem. Concr. Res.*, **15**[4] 675-80 (1985).
36. G. Engelhardt, J. Felsche, and P. Sieger, "The Hydrosodalite System  $\text{Na}_{6+x}[\text{SiAlO}_4]_6(\text{OH})_x \cdot n\text{H}_2\text{O}$ : Formation, Phase Composition, and De- and Rehydration Studied by  $^1\text{H}$ ,  $^{23}\text{Na}$ , and  $^{29}\text{Si}$  MAS-NMR Spectroscopy in Tandem with Thermal Analysis, X-ray Diffraction, and IR Spectroscopy," *J. Am. Chem. Soc.*, **114** 1173-82 (1992).

37. T. B. Douglas and J. L. Dever, "Anhydrous Sodium Hydroxide - The Heat Content from 0° to 700° C, the Transition Temperature, and the Melting Point," *J. Res. Nat. Bur. Stand.*, **53**[2] 81-90 (1954).
38. R. Dimitrijević, V. Dondur, and A. Kremenović, "Thermally Induced Phase Transformations of Ca-exchanged LTA and FAU Zeolite Frameworks: Rietveld Refinement of the Hexagonal CaAl<sub>2</sub>Si<sub>2</sub>O<sub>8</sub> Diphyllosilicate Structure," *Zeolites*, **16** 294-300 (1996).
39. T. Abe, K. sukamoto, and I. Sunagawa, "Nucleation, Growth and Stability of CaAl<sub>2</sub>Si<sub>2</sub>O<sub>8</sub> Polymorphs," *Phys. Chem. Miner.*, **17**[6] 473-84 (1991).
40. J. M. Rivas-Mercury, P. Pena, A. H. de Aza, and X. Turrillas, "Dehydration of Ca<sub>3</sub>Al<sub>2</sub>(SiO<sub>4</sub>)<sub>y</sub>(OH)<sub>4(3-y)</sub> (0<y<0.176) Studied by Neutron Thermodiffractometry," *J. Eur. Ceram. Soc.*, **28**[9] 1737-48 (2008).
41. P. Yu, R. J. Kirkpatrick, B. Poe, P. F. McMillan, and X. Cong, "Structure of Calcium Silicate Hydrate (C-S-H): Near-, Mid-, and Far-Infrared Spectroscopy," *J. Am. Ceram. Soc.*, **82**[3] 742-48 (1999).
42. S.-D. Wang, K. L. Scrivener, and P. L. Pratt, "Factors Affecting the Strength of Alkali-Activated Slag," *Cem. Concr. Res.*, **24**[6] 1033-43 (1994).
43. E. Balan, M. Lazzeri, G. Morin, and F. Mauri, "First-principles Study of the OH-Stretching Modes of Gibbsite," *Am. Mineral.*, **91**[1] 115-19 (2006).
44. S. Samal, A. K. Ray, and A. Bandopadhyay, "Proposal for Resources, Utilization and Processes of Red Mud in India — A review," *Int. J. Miner. Process.*, **118** 43-55 (2013).

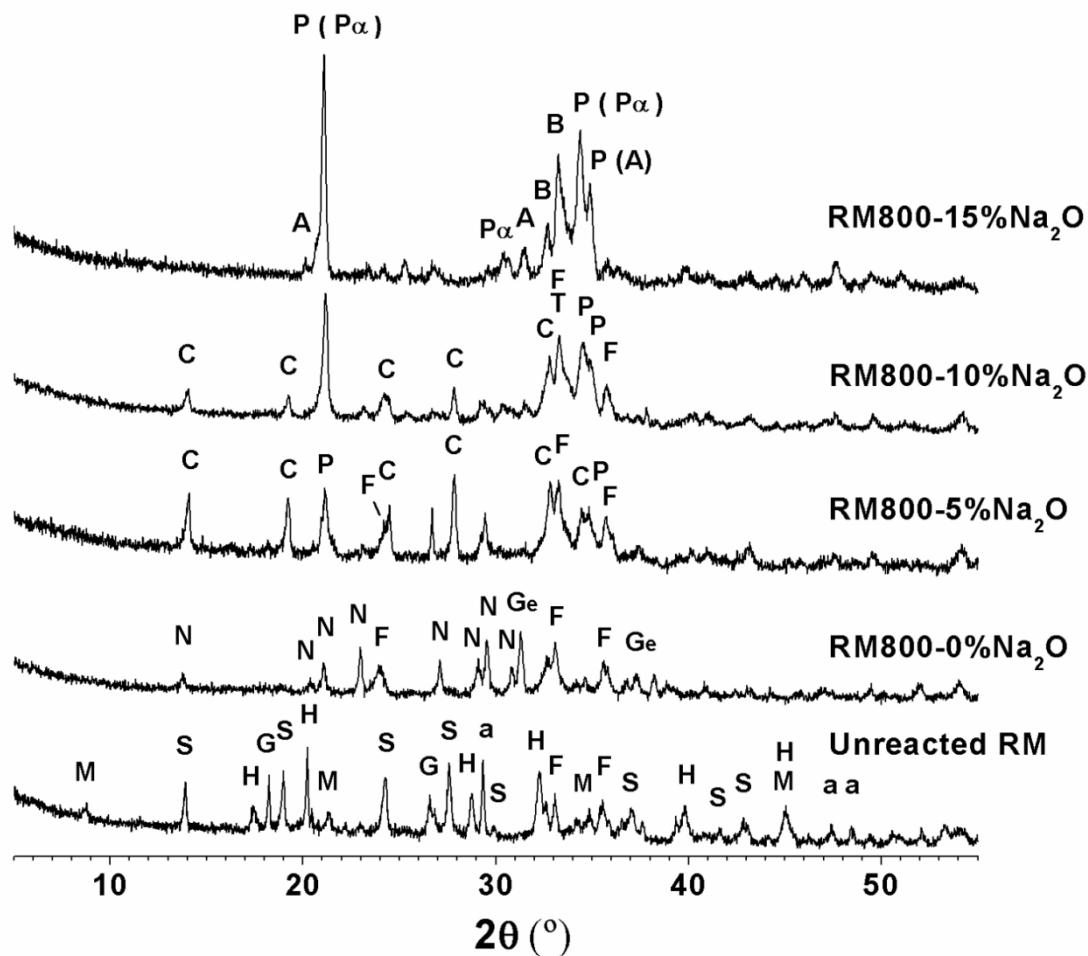
45. R. K. Paramguru, P. C. Rath, and V. N. Misra, "Trends in Red Mud Utilization – a Review," *Miner. Proc. Extr. Metall. Rev.*, **26**[1] 1-29 (2004).
46. V. J. Ingram-Jones, R. C. T. Slade, T. W. Davies, J. C. Southern, and S. Salvador, "Dehydroxylation Sequences of Gibbsite and Boehmite: Study of Differences between Soak and Flash Calcination and of Particle-Size Effects," *J. Mater. Chem.*, **6**[1] 73 (1996).
47. T. Bakharev, J. G. Sanjayan, and Y. B. Cheng, "Effect of Admixtures on Properties of Alkali-Activated Slag Concrete," *Cem. Concr. Res.*, **30**[9] 1367-74 (2000).
48. M. Handke and W. Mozgawa, "Vibrational Spectroscopy of the Amorphous Silicates," *Vib. Spectrosc.*, **5**[1] 75-84 (1993).
49. R. M. K. Sinko, J. Rohonczy, and P. Fratzl, "Gel Structures Containing Al(III)," *Langmuir*, **15** 6631-36 (1999).
50. M. Sitarz, M. Handke, and W. Mozgawa, "Identification of Silicoxygen Rings in SiO<sub>2</sub> Based on IR Spectra," *Spectrochim. Acta, Part A*, **56**[9] 1819-23 (2000).
51. S. Markovic, V. Dondur, and R. Dimitrijevic, "FTIR Spectroscopy of Framework Aluminosilicate Structures: Carnegieite and Pure Sodium Nepheline," *J. Mol. Struct.*, **654**[1-3] 223-34 (2003).
52. H. Zhao, Y. Deng, J. B. Harsh, M. Flury, and J. S. Boyle, "Alteration of Kaolinite to Cancrinite and Sodalite by Simulated Hanford Tank Waste and its Impact on Cesium Retention," *Clays Clay Miner.* **52**[1] 1-13 (2004).
53. B. O. Mysen and G. D. Cody, "Solution Mechanisms of H<sub>2</sub>O in Depolymerized Peralkaline Melts," *Geochim. Cosmochim. Acta*, **69**[23] 5557-66 (2005).

54. B. O. Mysen and D. Virgo, "Volatiles in Silicate Melts at High Pressure and Temperature: 1. Interaction between OH Groups and  $\text{Si}^{4+}$ ,  $\text{Al}^{3+}$ ,  $\text{Ca}^{2+}$ ,  $\text{Na}^+$  and  $\text{H}^+$ ," *Chem. Geol.*, **57**[3–4] 303-31 (1986).
55. B. O. Mysen and D. Virgo, "Volatiles in Silicate Melts at High Pressure and Temperature: 2. Water in Melts along the Join  $\text{NaAlO}_2\text{-SiO}_2$  and a Comparison of Solubility Mechanisms of Water and Fluorine," *Chem. Geol.*, **57**[3–4] 333-58 (1986).
56. C. E. White, J. L. Provis, A. Llobet, T. Proffen, and J. S. J. van Deventer, "Evolution of Local Structure in Geopolymer Gels: An In Situ Neutron Pair Distribution Function Analysis," *J. Am. Ceram. Soc.*, **94**[10] 3532-39 (2011).
57. J. L. Provis, G. C. Lukey, and J. S. J. van Deventer, "Do Geopolymers Actually Contain Nanocrystalline Zeolites? - A Reexamination of Existing Results," *Chem. Mater.*, **17**[12] 3075-85 (2005).
58. A. Fernández-Jiménez, M. Monzó, M. Vicent, A. Barba, and A. Palomo, "Alkaline Activation of Metakaolin–Fly Ash Mixtures: Obtain of Zeoceramics and Zeocements," *Micropor. Mesopor. Mater.*, **108**[1-3] 41-49 (2008).
59. R. R. Lloyd, "Accelerated ageing of geopolymers," pp. 139-66. in *Geopolymers: Structure, Processing, Properties and Industrial Applications*. Edited by J. L. Provis and J. S. J. Van Deventer. Woodhead, Cambridge, UK, 2009.
60. Y. Deng, J. B. Harsh, M. Flury, J. S. Young, and J. S. Boyle, "Mineral Formation during Simulated Leaks of Hanford Waste Tanks," *Appl. Geochem.*, **21**[8] 1392-409 (2006).

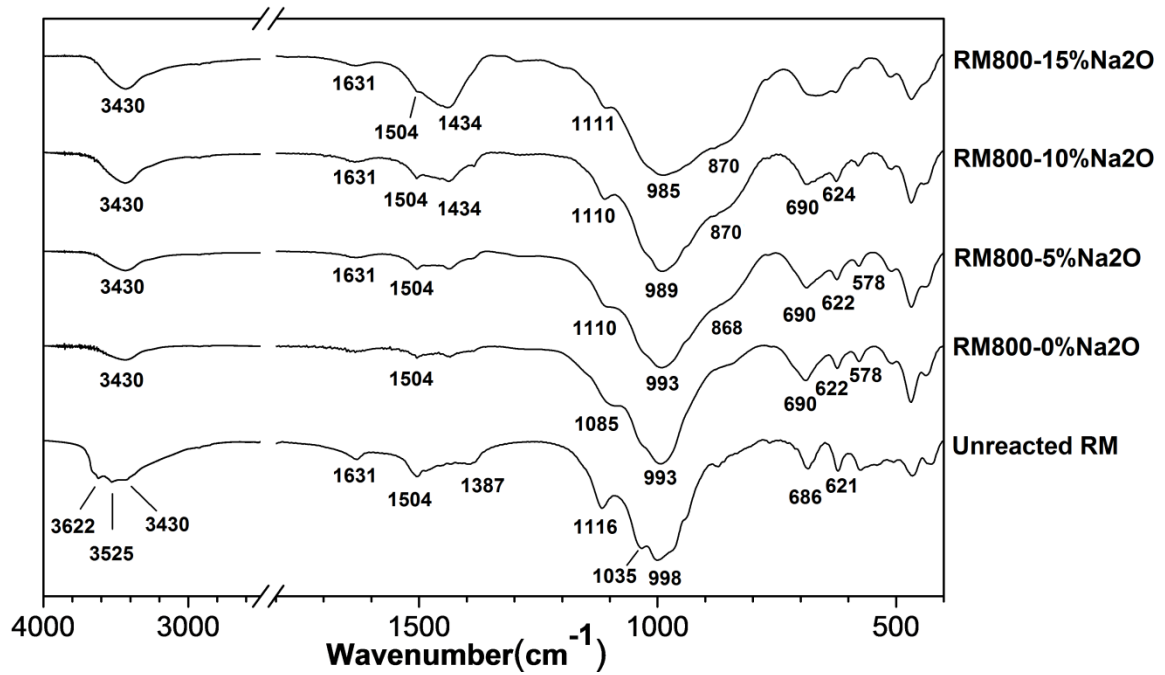
61. J. M. Rivas Mercury, X. Turrillas, A. H. de Aza, and P. Pena, "Calcium Aluminates Hydration in Presence of Amorphous SiO<sub>2</sub> at Temperatures below 90°C," *J. Solid State Chem.*, **179**[10] 2988-97 (2006).
62. C. H. Rüscher, E. Mielcarek, W. Lutz, A. Ritzmann, and W. M. Kriven, "Weakening of Alkali-Activated Metakaolin During Aging Investigated by the Molybdate Method and Infrared Absorption Spectroscopy," *J. Am. Ceram. Soc.*, **93**[9] 2585-90 (2010).
63. E. Najafi Kani, A. Allahverdi, and J. L. Provis, "Efflorescence Control in Geopolymer Binders Based on Natural Pozzolan," *Cem. Concr. Compos.*, **34**[1] 25-33 (2012).
64. P. Duxson, J. L. Provis, G. C. Lukey, S. W. Mallicoat, W. M. Kriven, and J. S. J. van Deventer, "Understanding the Relationship between Geopolymer Composition, Microstructure and Mechanical Properties," *Colloids Surf., A*, **269**[1-3] 47-58 (2005).

**Table 2.** Chemical composition of the red mud and slag used, determined via X-ray fluorescence analysis. LOI is loss on ignition at 1000°C

Component (wt.%)	SiO <sub>2</sub>	Al <sub>2</sub> O <sub>3</sub>	CaO	Na <sub>2</sub> O	K <sub>2</sub> O	Fe <sub>2</sub> O <sub>3</sub>	SO <sub>3</sub>	Others	LOI
Red mud	20.4	24.5	12.9	11.5	0.9	9.5	0.7	4.4	15.4

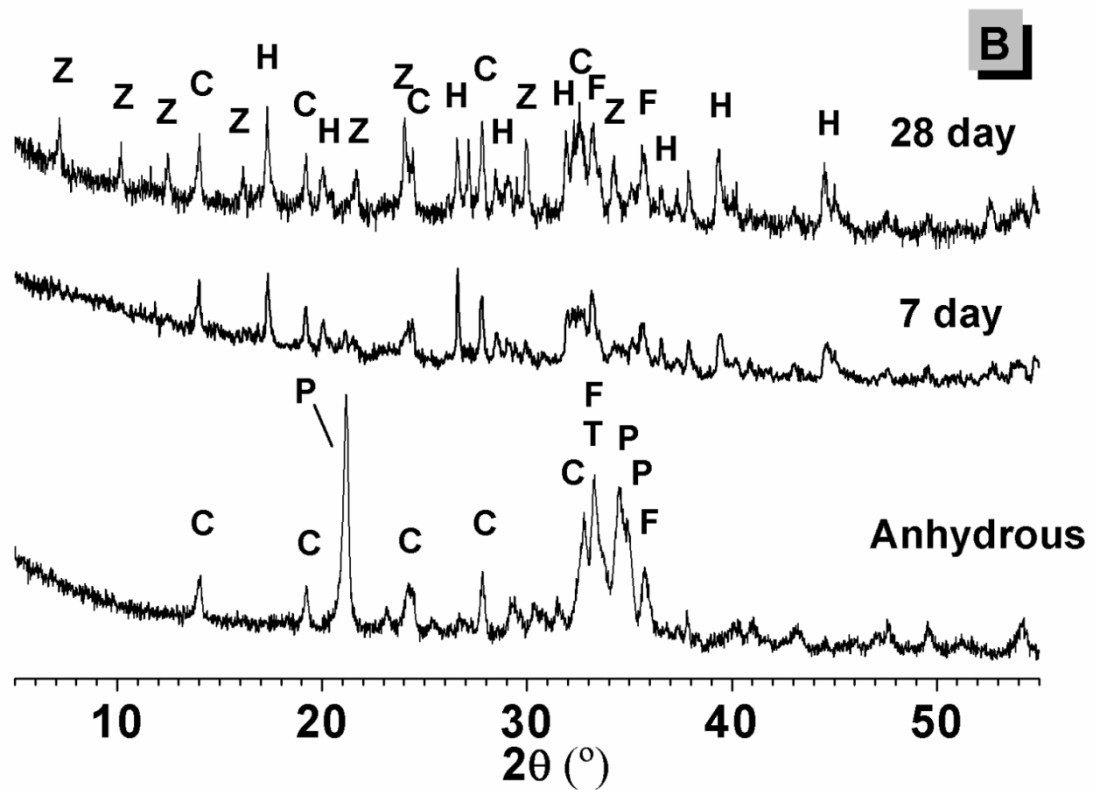
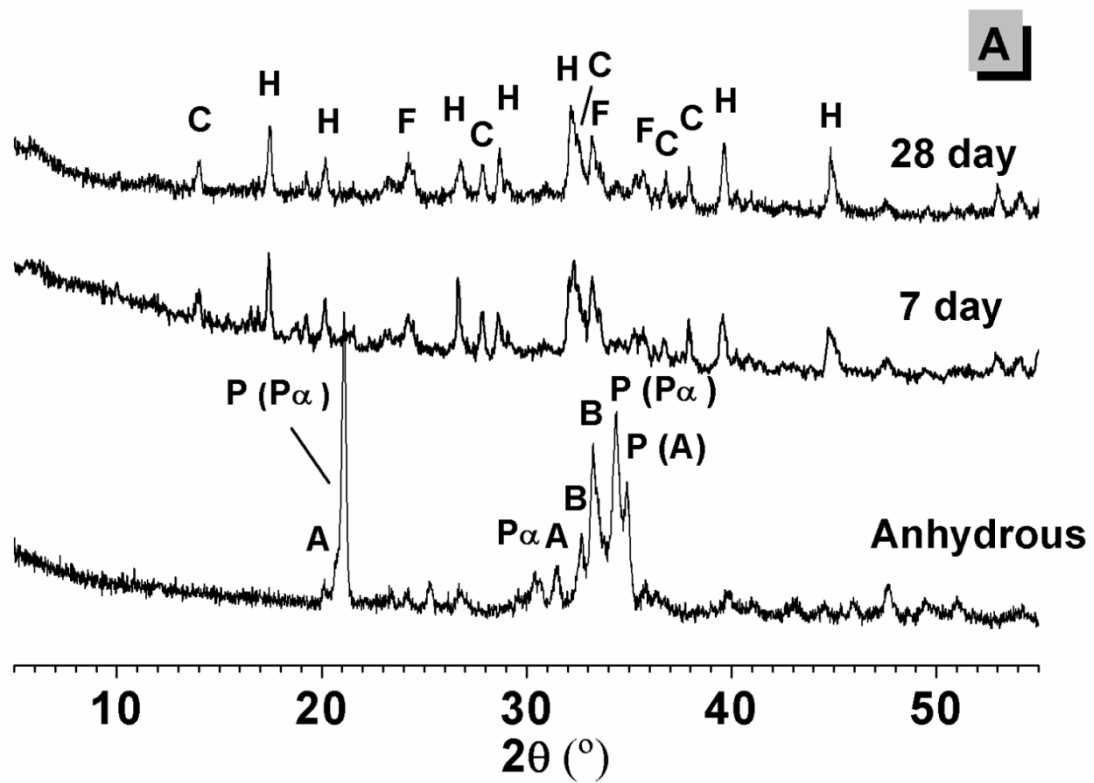


**Fig. 1** X-ray diffractograms of unreacted red mud and red mud binders prepared by thermally treated at 800°C incorporated with different amount of alkali. S - cancrisilite, H - hydrogarnet, G - gibbsite, M - muscovite, a - calcite, F - hematite, N - nepheline, Ge - gehlenite, P and P $\alpha$  – disordered peralkaline aluminosilicate, C –Ca-substituted cancrinite, T - tricalcium aluminate, A – hexagonal CAS<sub>2</sub>, B - belite.



**Fig. 2** FTIR spectra of unreacted red mud and alkali-incorporated thermally pre-activated red mud.





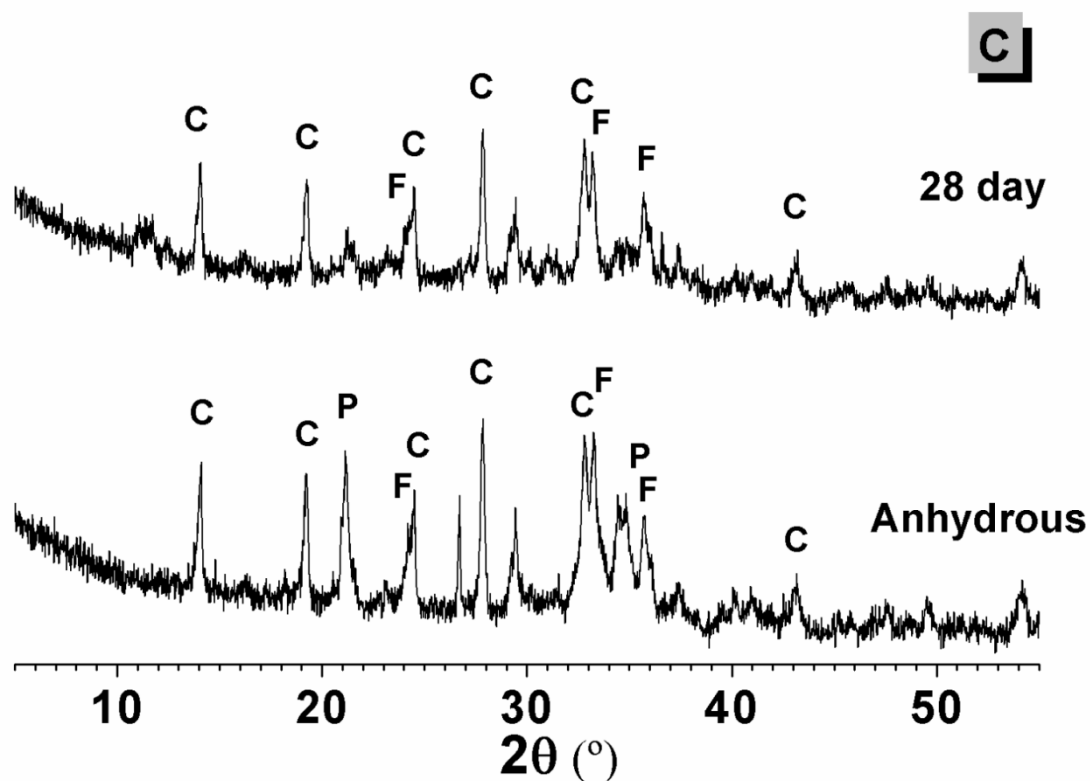


**Fig. 3** X-ray diffractograms of one-part geopolymer synthesised from alkali-thermal pre-activated red mud binder with (A) 15%Na<sub>2</sub>O, (B) 10%Na<sub>2</sub>O, (C) 5%Na<sub>2</sub>O over different days of curing. P and P<sub>α</sub> - peralkaline aluminosilicate, C - cancrinite, B - belite, F - hematite, Z - zeolite NaA, H - hydrogarnet, T - tricalcium aluminate, A – hexagonal CAS<sub>2</sub>.

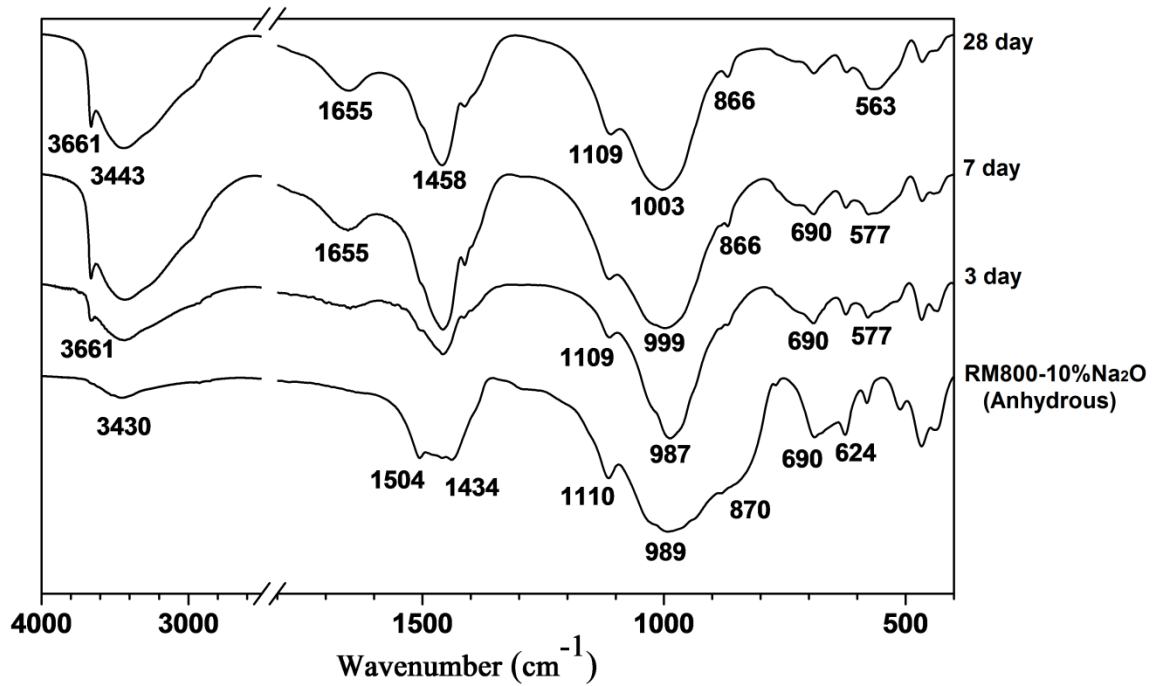


**Fig. 4** FTIR spectra of one-part geopolymer generated from R800-10%Na<sub>2</sub>O at different times of curing.

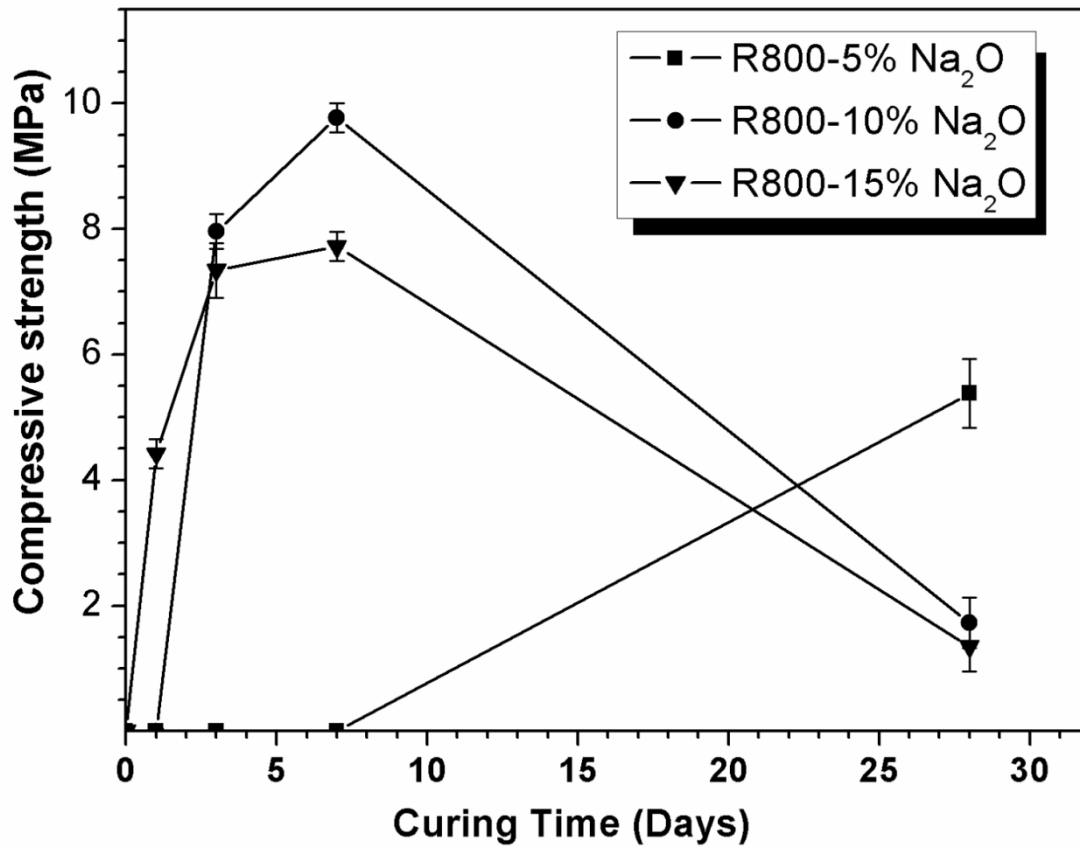


**Fig. 5** Compressive strengths of red mud based one-part geopolymers produced with different activator doses as a function of the time of curing.

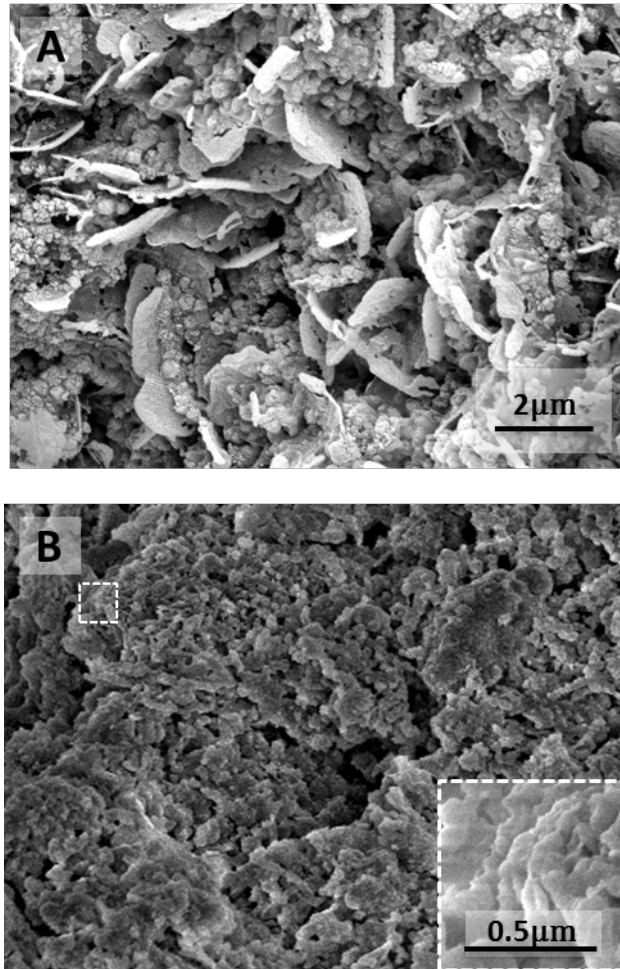


**Fig. 6** SEM micrographs of the fracture surface of one-part geopolymer generated from R800-10%Na<sub>2</sub>O after (A) 7 and (B) 28 days of curing.